Serial Clustering of Extratropical Cyclones

PASCAL J. MAILIER, DAVID B. STEPHENSON, AND CHRISTOPHER A. T. FERRO

Department of Meteorology, University of Reading, Reading, United Kingdom

KEVIN I. HODGES

Environmental Systems Science Centre, University of Reading, Reading, United Kingdom

(Manuscript received 9 May 2005, in final form 26 October 2005)

ABSTRACT

The clustering in time (seriality) of extratropical cyclones is responsible for large cumulative insured losses in western Europe, though surprisingly little scientific attention has been given to this important property. This study investigates and quantifies the seriality of extratropical cyclones in the Northern Hemisphere using a point-process approach. A possible mechanism for serial clustering is the time-varying effect of the large-scale flow on individual cyclone tracks. Another mechanism is the generation by one "parent" cyclone of one or more "offspring" through secondary cyclogenesis. A long cyclone-track database was constructed for extended October–March winters from 1950 to 2003 using 6-h analyses of 850-mb relative vorticity derived from the NCEP–NCAR reanalysis. A dispersion statistic based on the variance-to-mean ratio of monthly cyclone counts was used as a measure of clustering. It reveals extensive regions of statistically significant clustering in the European exit region of the North Atlantic storm track and over the central North Pacific. Monthly cyclone counts were regressed on time-varying teleconnection indices with a log-linear Poisson model. Five independent teleconnection patterns were found to be significant factors over Europe: the North Atlantic Oscillation (NAO), the east Atlantic pattern, the Scandinavian pattern, the east Atlantic–western Russian pattern, and the polar–Eurasian pattern. The NAO alone is not sufficient for explaining the variability of cyclone counts in the North Atlantic region and western Europe. Rate dependence on time-varying teleconnection indices accounts for the variability in monthly cyclone counts, and a cluster process did not need to be invoked.

1. Introduction

The development of severe extratropical cyclones over the North Atlantic can have devastating effects on the European economy, especially when these storms move over the continent. For instance, the three severe storms of December 1999 (Anatol, Lothar, and Martin[1]) cost an estimated 18.5 billion euros in economic damage, of which 10.7 billion was insured (Munich Re 2002). Such storms often develop rapidly and fail to head north before making landfall into Europe. The most damaging European storms generally belong to one or more of the following three types.

1) Serial storms: These storms typically occur when successive unstable waves develop and move rapidly along the trailing front in the wake of a large "parent" low. The two devastating storms of Christmas 1999, Lothar and Martin, were separated by just a 36-h interval. Several episodes with consecutive storms have caused large insured losses in recent years, notably the eight storms in December 1989 and January 1990 (10.5 billion euros), and the three storms in December 1999 (10.7 billion euros). The seriality of European winter storms during a season can lead to cumulative insurance losses comparable to those from a catastrophic hurricane.
2) Rapid developers: Fast developments leading to

[1] Since 1954, the Institute for Meteorology at the *Freie Universität* Berlin has given names to all extratropical cyclones and anticyclones that influence the weather in Europe. Highs and lows are assigned names of opposite genders. The names are in alphabetical order, and genders alternate every year (more information available online at http://www.met.fu-berlin.de/wetterpate/).

Corresponding author address: Pascal Mailier, Department of Meteorology, University of Reading, Earley Gate, P.O. Box 243, Reading RG6 6BB, United Kingdom.
E-mail: p.j.a.mailier@reading.ac.uk

very deep cyclones are not exceptional in the North Atlantic storm track. Extratropical cyclones with deepening rates exceeding 24 hPa day^{-1} are known as *explosive cyclones* or "*bombs*" (Bergeron 1954). Deepening at over twice that rate is not uncommon in winter over the North Atlantic and the North Pacific. There is evidence that the number of explosive cyclones has increased globally over the past 21 yr and 45 bombs yr^{-1} occur on average in the Northern Hemisphere (Lim and Simmonds 2002). Fortunately, many of these cyclones reach Europe in a late stage of their life cycle and they do not intensify further (e.g., the Baltic storm of January 1993, the English Great Storm of October 1987, and the storms of December 1999).

3) Slow movers: Because they move slowly, these systems are able to produce large accumulations of precipitation concentrated over small regions and so can lead to serious flood damage such as the storm of 14–15 November 2002, which caused severe flooding in eastern Scotland.

This study will focus on serial storms. Besides the obvious economic motivation, serial clustering of extratropical cyclones raises several challenging scientific questions:

- How can the serial clustering of extratropical cyclones be quantified?
- Do extratropical cyclones cluster more than expected by chance?
- What are the key mechanisms behind seriality?
- How predictable is cyclone seriality?
- Will cyclone seriality increase in the future?

Previous studies on midlatitude storm tracks (e.g., Hoskins and Hodges 2002, and references therein) have already presented descriptive diagnostic statistics of track and feature densities, but have not addressed the issue of seriality. There is an obvious need to develop probabilistic model-based approaches for quantifying the effect that cyclone seriality has on risk in the northeastern Atlantic and Europe. Specifically, ignoring important variations in the rate of storms may lead to a significant underestimation of storm-related risks.

This introductory paper on seriality deals with the first three essential questions above. Section 2 of this paper presents the dynamical background on cyclone seriality. Although clustering was recognized early on as a property of extratropical cyclones, and despite the societal impact mentioned above, it has received little attention in the published scientific literature. Section 3 provides a description of the meteorological dataset used and an explanation of how the cyclonic features were identified and tracked. In section 4, the stochastic Poisson process model used to assess clustering is described. The mathematical derivations are presented in the appendix. Section 5 presents results for the Northern Hemisphere, but with particular emphasis on the North Atlantic and European sectors. Section 6 summarizes the main findings and suggests possible future work.

2. Background

a. Complete serial randomness

A useful statistical tool to model the succession of events such as cyclone occurrences at a particular location is the *point process* (see Cox and Isham 1980 for a detailed discussion). The simplest hypothesis that can be formulated is that cyclones occur in a completely random fashion (i.e., the occurrence of one cyclone at any moment is independent of previous occurrences). In this case the occasional time aggregation of extratropical cyclones is only due to chance. The simplest model that describes complete serial randomness is the one-dimensional *Poisson process with constant intensity* (*or rate*), also known as the *simple homogeneous Poisson process*. A more complete description of this process and its properties is given in the appendix.

However, cyclones affect the ambient baroclinicity of the storm track (e.g., through diabatic heating; Hoskins and Valdes 1990), so it is reasonable to think of possible dependencies that may cause the cyclones to occur either in clusters, or at more regular intervals.

b. Serial clustering

One possible mechanism for clustering is the time-varying effect of large-scale factors on individual cyclone tracks. The variable frequency of cyclone occurrence that results can produce apparent clusters of events during periods when the rate is high. A point process that models this mechanism is the *Poisson process with variable rate*, also known as the *inhomogeneous Poisson process*. Situations featuring a strong jet stream across the North Atlantic are often associated with a fast succession of baroclinic waves due to a vigorous steering flow, and the enhanced baroclinicity provides favorable conditions for the formation and growth of frontal waves. Strong upper-level divergence and vertical ascent at the right entrance and left exit of jet streaks[2] (Namias and Clapp 1949; Murray and

[2] Regions of wind speed maxima embedded within jet streams (Palmén and Newton 1969).

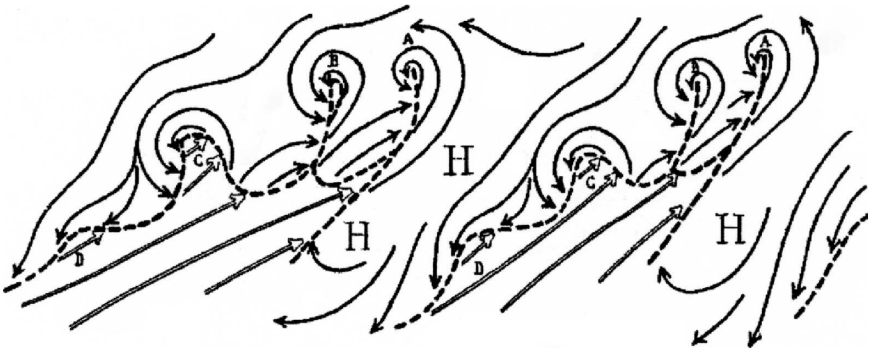

FIG. 1. Cyclone families in the storm track: in this model, a secondary cyclone is formed on the waving cold front of a primary parent cyclone. The new cyclone is dynamically similar to its parent. From Bjerknes and Solberg (1922).

Daniels 1953) contribute to the rapid development of extratropical cyclones and severe storms (Uccellini and Johnson 1979; Uccellini 1990). In the North Atlantic, strong jet streams and high cyclone rates are observed when the Icelandic low is deeper and the Azores high is stronger than normal [i.e., when the North Atlantic Oscillation (NAO) is in a positive phase]. For this reason, the NAO has traditionally been regarded as the principal large-scale pattern that explains the variation in the rate of cyclones arriving in western Europe (Rogers 1997). However, little attention has been devoted to the possible contribution of other large-scale factors besides the NAO.

A process with a fluctuating rate is not the only source of clustering. Cyclones may also be clustered in space and time because they form part of a coherent entity such as a wave packet. A point process that models this behavior is known as a *Poisson cluster process*. An example of this type of process is when the occurrence of one parent event triggers the occurrence of one or more "offspring." This is a key idea in the early model of *cyclone families* proposed by the *Bergen School* (Bjerknes and Solberg 1922). The cyclone family model relied on the assumption of a preexisting *polar front*—a discontinuity surface separating the cold polar air from the warm tropical air. Waves are produced as a result of the inherent instability of the polar front and then propagate along this front as "families" of cyclones, with each cyclone in the family being seen as a replica of the preceding cyclone at an earlier stage of its cyclonic development (Fig. 1). Each family of cyclones brings warm and moist air from the south, and is separated from the following family by an incursion of cold polar air from the higher latitudes. Numerical simulations of the atmospheric general circulation led later to the understanding that "primary cyclones," or, in family parlance "parent cyclones" can themselves create fronts along which new, generally smaller "secondary" cyclones may form (Eliassen 1966).

Simmons and Hoskins (1979) proposed that the cyclone family might be seen as a manifestation of upstream energy dispersion along the trailing cold front behind a parent cyclone. This idea was reexamined by Thorncroft and Hoskins (1990) in a paper on frontal cyclogenesis. Furthermore, Simmons and Hoskins (1979) and later Orlanski and Chang (1993) pointed out that baroclinic waves can also develop through downstream propagation of energy. In contrast with the Bergen School cyclone family, offspring in a wave packet are generated ahead of the parent cyclone, as the energy propagates downstream at over twice the speed of the waves. Chang and Orlanski (1993, 1994) emphasized the important role of downstream energy dispersion (downstream developments) from baroclinic waves in extending eddy activity eastward in the less baroclinic regions of the northern Pacific storm track.

It is not obvious that a simple cluster process can be used to describe cyclone clustering. This is due to the complexity and variety of mechanisms that govern fronts and cyclones. Distinct types of midlatitude cyclones have been identified according to their mode of formation (Charney 1947; Eady 1949; Petterssen 1956; Petterssen and Smebye 1971; Deveson et al. 2002), and cyclones that belong to the same cluster may not necessarily share the same structure and origin (e.g., baroclinic instability, extratropical transition of a tropical cyclone, upper-level advection of vorticity). Parker (1998) even argued that, in view of their smaller scale, secondary frontal waves are subject to a wider range of mechanisms that can then affect their growth. The combination of mechanical factors (e.g., flow deformation) and physical processes (e.g., latent heat release) contribute to increasing cyclone heterogeneity (e.g., Renfrew et al. 1997; Mallet et al. 1999). We can reasonably

assume, however, that observed cyclone clusters are likely to be produced by a combination of inhomogeneous and cluster processes, and that the resulting compound clustering must be accounted for by modes of climate variability that have lower frequencies than the synoptic scale.

c. Serial regularity

Rather than clustering, the other alternative to pure serial randomness is regularity of cyclone occurrences. A natural cause for regular patterns is the existence of minimum permissible distance and time between any two events. Extratropical cyclones are not points, but have horizontal length scales that range typically from several hundreds to more than one thousand kilometers. The centers of successive cyclones cannot be indefinitely close, and as a result we may expect some regularity to arise where the process has very high rates. Another possible reason for regularity is that baroclinic waves can be more regular in the early stages of their growth than when these waves become predominantly nonlinear at larger amplitude farther downstream.

3. Cyclone track database

a. Data

A long climatology of Northern Hemisphere storm tracks has been computed using 53 extended winters (October–March 1950/51–2002/03) of 6-h reanalyses from the National Centers for Environmental Prediction–National Center for Atmospheric Research (NCEP–NCAR) reanalysis (Kalnay et al. 1996). The choice of the NCEP–NCAR reanalysis is motivated by the following reasons.

1) It is the longest reanalysis product available at a 6-h sample rate.
2) It is freely accessible at the NOAA–Cooperative Institute for Research in Environmental Sciences (CIRES) Climate Data Center, Boulder, Colorado (more information available online at http://www.cdc.noaa.gov/).
3) A recent comparison with other reanalyses including the European Centre for Medium-Range Weather Forecasts (ECMWF) 15-yr Re-Analysis (ERA-15; Hodges et al. 2003) showed little difference overall in the tracking statistics for a broad range of fields at lower-tropospheric levels.

Previous studies have often used the conventional December–February (DJF) winter season. For example, Hoskins and Hodges (2002) used only 21 DJF winters (1979–2000). This study has used instead extended winter seasons lasting October–March (ONDJFM) in order to avoid missing the cyclones that occur in the autumn and early spring. The new track dataset here has been computed using 53 October–March winters, which makes it the longest objective track dataset to be studied.

The zonal and meridional components of the 850-mb wind were extracted for the whole Northern Hemisphere. The 850-mb wind components were then used to compute the 850-mb relative vorticity ξ_{850}. Although mean sea level pressure (SLP) has historically been the traditional variable used for tracking cyclones, ξ_{850} is better able to detect cyclones because this variable focuses on smaller spatial scales and it is less influenced by the background state than SLP. Systems with a cyclonic circulation around a maximum of relative vorticity can often be located in the early stages of their development long before the associated minimum in surface pressure is detectable (i.e., systems at an open wave stage with no closed isobars, see, e.g., Sinclair 1994). Relative vorticity also gives a measure of the circulation around the cyclone, and so is more directly associated to the two physical variables that cause damage: wind (through circulation) and precipitation (through vertical motion). One potential drawback of relative vorticity is that it is spatially more noisy than SLP because it resolves mesoscale structures such as fronts. However, this does not appear to be a problem at the relatively low horizontal resolution (T63) of the NCEP–NCAR reanalysis.

b. Identification and tracking of cyclones

Early methods for tracking cyclones were predominantly subjective (e.g., Klein 1957; Akyildiz 1985; Reed et al. 1986). A major inconvenience of subjective tracking is the limitation of the geographical region explored and of the number of phenomena that can be followed. However, the need to deal with increasingly large meteorological datasets and the availability of better computer technology have stimulated the development of various automated feature-tracking systems. The simplest and most common algorithms are based on nearest-neighbor searches (e.g., Blender et al. 1997). Unfortunately nearest-neighbor searches may produce inconsistent results when dealing with fast-moving features or when the elapsed time between consecutive analysis frames is large. More sophisticated techniques were developed in order to address these deficiencies. For example, Murray and Simmonds (1991) devised a local optimization scheme to identify low pressure centers, and then computed the tracks by calculating the probability of association between the features. The method was refined later by Simmonds et al. (1999) and com-

pared against manual tracking. They found that in general the automatic algorithm tended to find more systems than the manual analysis, the extra systems being mainly those identified as weak or open. Simmonds and Keay (2000) applied this method in a study of extratropical cyclones in the Southern Hemisphere.

Other tracking algorithms have been developed and used to study cyclone activity (e.g., Serreze 1995; Serreze et al. 1997). The cyclone tracks here have been calculated using the objective technique developed by Hodges (1994, 1995, 1996). This scheme has already been successfully employed in several previous studies (e.g., Hoskins and Hodges 2002; Hodges et al. 2003). The approach proceeds as follows:

1) Filter out the planetary-scale background waves. For this work, spherical harmonics with wavenumber $n \leq 5$ have been removed from the original fields as recommended by Hoskins and Hodges (2002). Although this step is not so much required on ξ_{850} fields as it is on SLP fields, it ensures that the local minima or maxima to be tracked are not confounded by planetary wave factors (Anderson et al. 2003).
2) Identify the ξ_{850} cyclonic features. The data are interpolated or smoothed using a spline technique for the sphere. This method provides surface fits with continuity constraints so that the surface is periodic in longitude and continuous at the poles. Taking the gridpoint maxima as starting points, the off-grid position and field value of the local maximum are then found by means of a constrained conjugate gradient method (Goldfarb 1969). The weakest features (local ξ_{850} maxima less than 10^{-5} s^{-1}) are ignored to help improve the efficiency of the tracking without losing the features of interest.
3) Tracking: This operation is performed directly on a sphere to overcome the problems caused by the unavoidable distortion errors that arise with projections (Hodges 1995; Hoskins and Hodges 2002). Following Hodges (1994), the correspondence between the feature points in successive frames was determined by using the constrained optimization of a cost function. The main constraint is on *path coherence* (i.e., the motion of objects cannot change discontinuously in speed and direction). The smoothest possible set of trajectories is obtained by minimizing a cost function that expresses the local deviations of the tracks using the positions of feature points in three consecutive time steps. A detailed explanation of the cost function is given in Hodges (1994, 1995). For each track, the local deviation is calculated in terms of the change in displacement and direction measured over three time steps (there is no penalty if the three points are collinear and if the displacements between successive points are equal). The cost to be minimized is then the sum of the local deviations over all the tracks, subject to constraints on the displacement and track smoothness, which are applied adaptively (Hodges 1999). The maximum-displacement constraint is relaxed over oceanic regions in order to capture extreme cases of exceptionally fast features. The tracks are initialized using the nearest-neighbor distance algorithm.

It takes several days for an extratropical cyclone to go through its entire life cycle. In this analysis, only the tracks that lasted for at least 48 h were selected as true cyclone tracks. A total number of 48 818 tracks were retained for the analysis.

c. *Inspection of the tracks*

The ξ_{850} tracks of some well-known cases of severe extratropical cyclones were plotted and compared against corresponding tracks based on SLP minima. Examination of the tracks revealed a small (typically less than 100 km) southerly shift of the ξ_{850} tracks relative to the SLP tracks. The maximum of relative vorticity did not generally coincide with the corresponding minimum of mean sea level pressure. These differences are mainly due to the latitudinal variation of the planetary vorticity (Coriolis parameter) and the increased cyclonic shear in the frontal regions in the southern half of the low pressure systems.

As expected ξ_{850} gave a better detection of the systems in the early stages of their development. A comparison of ξ_{850} and SLP tracks for the storms of December 1999 is shown in Fig. 2.

4. Stochastic modeling of cyclone transits

The need of a discrete distribution and the point-process argument made in section 2 lead naturally to using the Poisson distribution as a basis for modeling cyclone counts. Incorporating over- and underdispersion is a standard extension of the Poisson regression that is useful here. An alternative distribution for modeling overdispersed counts is the negative binomial distribution (McCullagh and Nelder 1989, chapter 6).

A regular grid covering an area 10°–80°N and 170°W–180° provided a set of reference points. A 5° spatial resolution permits reasonably smooth fields while keeping computer-processing time to a minimum. At each of these grid points, cyclone tracks crossing the local meridian within ±10° of latitude from the point were counted. A latitude bandwidth of 20° was found

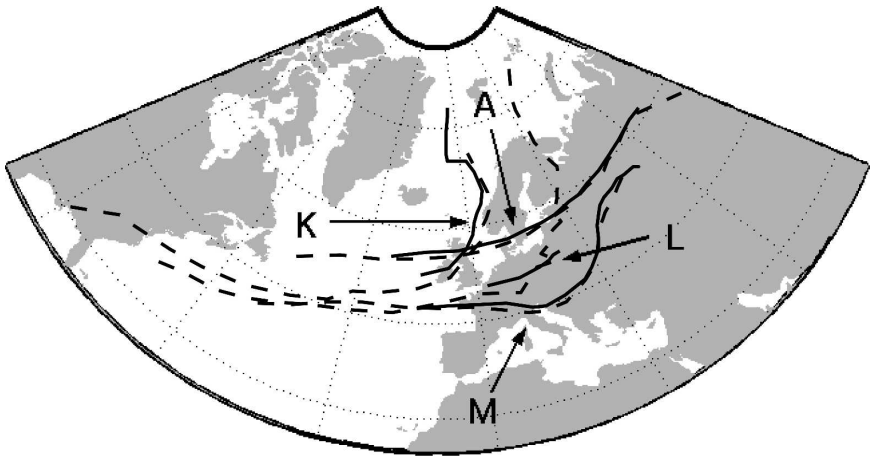

FIG. 2. Tracks of the four strongest European storms of December 1999: Anatol (A; 3–4 Dec), Kurt (K; 24–25 Dec), Lothar (L; 26 Dec), and Martin (M; 27–28 Dec). The solid lines show the tracks based on SLP, the dashed lines the tracks based on ξ_{850}.

narrow enough for conditions 1) and 2) of the Poisson process to hold (see the appendix), and also wide enough to take account of the typical length scale of extratropical cyclones, which is between 1000 and 2000 km. Only the first transits of eastward-moving cyclones were counted in order to exclude easterly waves and avoid multiple counts of recurving features. For each event, the time and relative vorticity at the moment of transit were recorded. The total number N of transits for each month was evaluated at each grid point.

The probability distribution of the monthly counts N has been modeled as a Poisson distribution with mean number of transits μ given by Eq. (A3) in the appendix:

$$N \mid \mu \sim \text{Poisson}(\mu),$$

where $\sim$ means *distributed as* and $\mid \mu$ means *given* μ.

The mean number of transits μ has been related to the large-scale flow using the log-linear relationship of Eq. (A4) in the appendix:

$$\ln(\mu) = \beta_0 + \sum_{k=1}^{p} \beta_k x_k.$$

The x_k variables are 10 indices and 5 binary variables ($p = 15$) that quantify the mean state of the large-scale atmospheric flow for each month.

The use of a Poisson distribution here stems from the Poisson process argument made in section 2a [i.e., that the most natural assumption (null hypothesis) when dealing with random events is that of complete randomness]. Furthermore, we need a discrete distribution to model counts, which are inherently nonnegative integers. Incorporating overdispersion is a standard extension of the Poisson regression that is useful here. The indices used for this analysis were monthly teleconnection indices for the Northern Hemisphere calculated by the Climate Prediction Center (CPC). (These data can be freely downloaded from the CPC Web site at ftp://ftpprd.ncep.noaa.gov/pub/cpc/.)

Rotated Principal Component Analysis (RPCA) was used at CPC to identify the teleconnection patterns (Barnston and Livezey 1987). RPCA was applied to monthly mean 700-mb geopotential height anomalies between January 1964 and July 1994. For every month of the year, the 10 most prominent patterns—the 10 leading empirical orthogonal functions (EOFs)—were selected. The reader is referred to Panagiotopoulos et al. (2002) for a detailed review and discussion of the Northern Hemisphere wintertime teleconnection patterns. Each month, CPC calculates the amplitudes of the 10 teleconnection patterns corresponding to that calendar month as the values that maximize the explained part of the geopotential height anomalies. The amplitudes are each standardized to have zero mean and unit variance. A list of the 10 teleconnection indices used in the analysis is given in Table 1. Teleconnection patterns that are not one of the 10 leading EOFs during a given month are considered inactive, and in the model the value of the corresponding x_k was set to zero for that month. By definition, teleconnection indices are not correlated with one another. This property makes them particularly suitable for use as explanatory variables in the Poisson regression.

In addition to the 10 teleconnection patterns, we

TABLE 1. Teleconnection indices used in the Poisson regression model. The values of the indices were set to zero for months during which the corresponding teleconnection pattern is considered to be inactive.

k	Teleconnection indices	$x_k = 0$
1	NAO	
2	EAP	
3	SCP	
4	East Atlantic–west Russia pattern	
5	Polar–Eurasian pattern	Oct, Nov, Mar
6	PNA pattern	
7	West Pacific pattern	
8	East Pacific pattern	
9	North Pacific pattern	Oct–Feb
10	Tropical Northern Hemisphere pattern	Oct, Feb, Mar

have also included seasonality in the model in the form of 5 binary indicator variables for each month from October to February. A sixth indicator variable for March is redundant because its state (0 or 1) is fully determined by the states of the other five.

The parameter β_0 corresponds to $\ln(\mu)$ for March with all teleconnection indices set to zero. Other parameters measure the dependence of the mean number of transits μ on the explanatory variable x_k. For example, β_1 gives the change in $\ln(\mu)$ accounted for by a unit standard deviation change in NAO.

5. Results

a. Clustering and regularity

Figure 3 shows the 53-winter mean $\overline{n}$ of the monthly totals n_i of cyclone transits past the 20° meridional section centered at every grid point on the 5° grid. The North Pacific and North Atlantic storm tracks can be clearly recognized, and qualitatively agree with the track density maps in Hoskins and Hodges (2002). The maxima in the westernmost parts of the two oceanic basins in Fig. 3 correspond to particularly intense baroclinic developments over the warm waters of the Gulf Stream (in the North Atlantic) and the Kuroshio (in the Pacific). These areas exhibiting high transit rates and explosive cyclogenesis were discussed in several previous studies: Petterssen (1956), Sanders and Gyakum (1980), Roebber (1984), and more recently by Lim and Simmonds (2002). The second maximum discernible in Fig. 3 in the central North Pacific is associated with the region of secondary development discussed by Roebber (1984) and Hoskins and Hodges (2002). There are also the well-known local maxima on the eastern (lee) side of the Rocky Mountains and in Siberia (Hoskins and Hodges 2002).

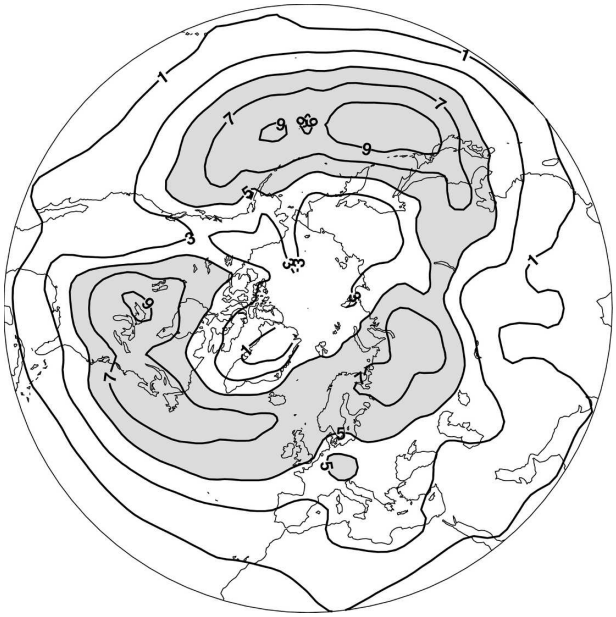

FIG. 3. Sample mean $\overline{n}$ of the monthly counts of cyclone transits. Contours start at 1 month^{-1}, contour intervals of 2 month^{-1}. Regions where $\overline{n} \geq 5$ month^{-1}, are shaded to highlight the storm tracks.

Figure 4 shows the 53-winter variance s_n^2 of the monthly transit counts. The variance is very similar to the mean shown in Fig. 3. In fact, the plots would have been identical to within sampling variation if the cyclone counts had been produced by a homogeneous

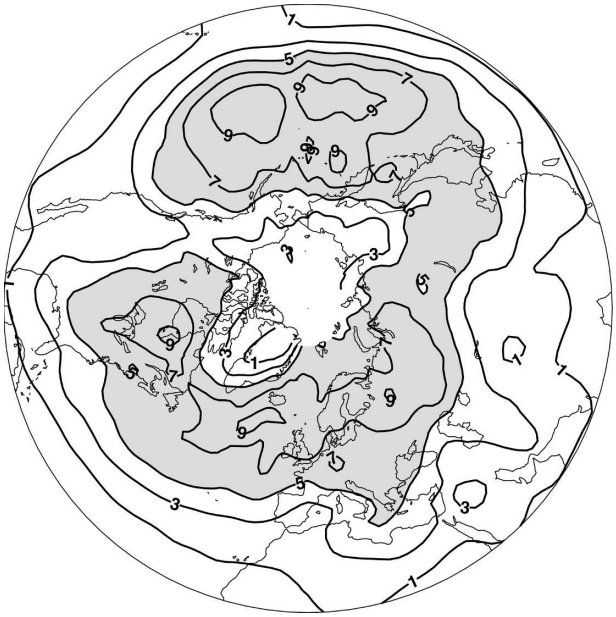

FIG. 4. Sample variance s_n^2 of the monthly number of cyclone transits. Contouring and shading as in Fig. 3.

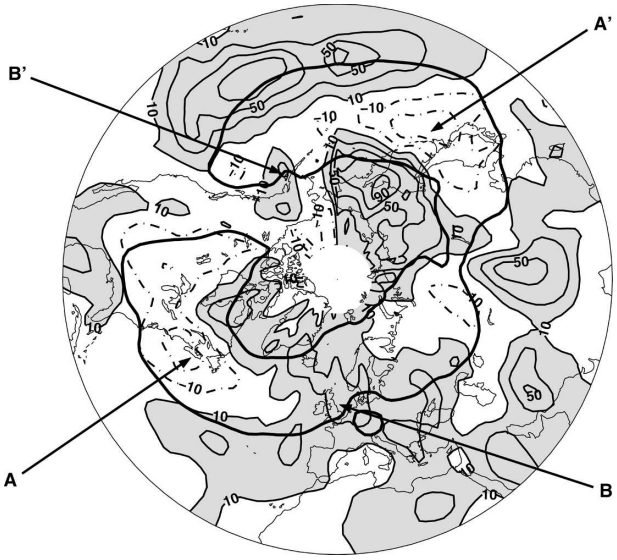

FIG. 5. Estimated dispersion statistic $\hat{\psi}$ (%) of the monthly number of cyclone transits. Solid (dashed) lines indicate positive (negative) values. Contours start at ±10%, contour intervals of 20%. Areas where $\hat{\psi} \geq 10\%$ are shaded. Thick dark lines representing the boundaries of the regions where $\bar{n} \geq 5$ month^{-1} (shaded areas in Fig. 3) have been added for easy reference to the storm tracks. For annotations A, B, A′, B′ see text.

Poisson process (see the appendix). Regions where the variance exceeds the mean can be noted in the eastern Atlantic region and Europe, and also in the central Pacific. In the western Atlantic and Pacific Oceans, where the highest mean transit counts occur, the variance is less than the mean. Over the oceans, the local maxima in the variance are located farther eastward than the corresponding local maxima in the mean. Over North America and Siberia the maxima coincide better, but the maxima in the variance are systematically lower than the corresponding maxima in the mean.

Figure 5 shows estimates of the dispersion statistic derived from Eq. (A10) in the appendix:

$$\hat{\psi} = \hat{\phi} - 1 = \frac{s_n^2}{\bar{n}} - 1. \qquad (1)$$

This statistic highlights the discrepancies between the mean and the variance of the monthly transit counts. Near-zero values of $\hat{\psi}$ are consistent with a purely random process with constant rate. Positive values of $\hat{\psi}$ (shaded regions with solid contours) indicate overdispersion in the distribution of the monthly transit counts, and are consistent with a process that is more clustered than a purely random process with a constant rate. Negative values indicate underdispersion, and are consistent with a process that is more regular than a purely random process with a constant rate. Focusing attention on the storm tracks, one can note striking similarities between the North Atlantic and North Pacific sectors. Both sectors exhibit enhanced underdispersion at the western end (entrance) of the storm track. There is evidence of overdispersion at the eastern end (exit) of the North Atlantic storm track. This is not surprising from synoptic experience. The northeastern Atlantic is typically the site of occluded cyclones, which tend to move slower and group together. However, overdispersion in this region also includes serial clusters of younger, fast-moving cyclones. There are other regions with pronounced overdispersion in central Asia, northeast Siberia and Kamchatka, and in the central Pacific. These regions are not of particular importance in the context of this study as they are situated off the storm tracks.

TABLE 2. Approximate critical values $\hat{\psi}_c$ (%) for estimates of the dispersion statistic $\hat{\psi}$. The α values in the first column give the probabilities that $|\hat{\psi}| > |\hat{\psi}_c|$ when $\psi = 0$ (no under/overdispersion). The symmetry of the critical regions (±) is due to the normal approximation.

α	$\hat{\psi}_c$ [%]
0.100	±10.2
0.050	±13.1
0.010	±18.5
0.005	±20.5
0.001	±24.5

The statistical significance of these results can be assessed from the critical values for $\hat{\psi}$ presented in Table 2. The critical values $\hat{\psi}_c$ were calculated using the normal approximation to the χ^2 distribution on 317 degrees of freedom given in the appendix ($m = 318$ and $p = 0$).

The different behaviors in the eastern and western North Atlantic storm track are illustrated further in Figs. 6 and 7. Figure 6a shows the times of transit of cyclones across a 20° strip of meridian centered at the grid point 45°N, 60°W (western Atlantic location A in Fig. 5) from December 1990 to March 1991. Figure 6b shows the observed transit times during the same period at the other end of the North Atlantic storm track at the grid point 55°N, 0° (eastern Atlantic location B in Fig. 5). Analogs exist in the North Pacific (locations A' and B' in Fig. 5), but the discussion will focus on the North Atlantic.

The transit times at location A clearly show more regularity than what would be expected from a simple random process with a constant rate. The transit times at location B reveal a more clustered pattern than could be accounted for by pure chance. Figures 7a,b show histograms for the distribution of monthly transit counts at each location over all 53 winters. The curves indicate the Poisson distributions that would be ob-

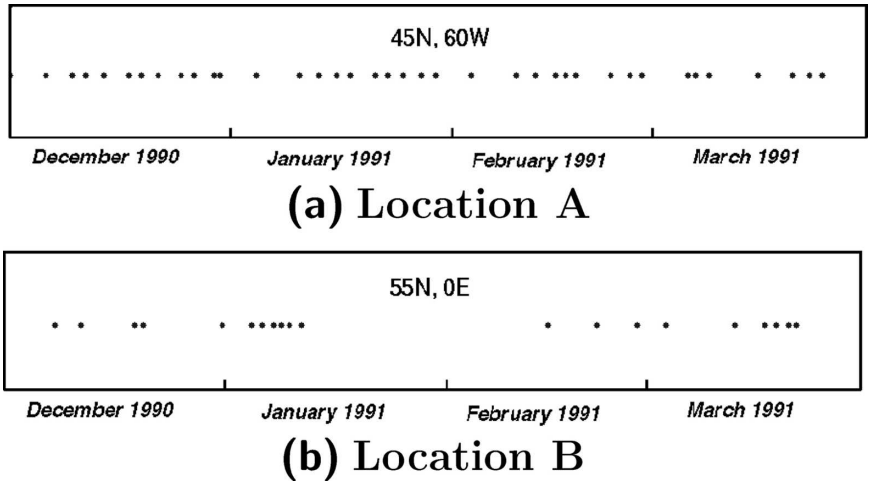

FIG. 6. Point processes describing the transits of cyclones at the entrance (location A) and at the exit (location B) of the North Atlantic storm track from December 1990 to March 1991.

tained for homogeneous Poisson processes. The sample means at points A and B were used to fit the Poisson distributions. In Fig. 7a the underdispersion (regularity) of the process at A can be seen by the spread of the histogram, which is smaller than the spread from the corresponding homogeneous Poisson process. Conversely, there is larger spread in the histogram in Fig. 7b, which is consistent with overdispersion (clustering) at B. Notice that although the histograms show larger average counts in A than in B, the maximum count is larger in B than in A.

The high rate and regular character of the process in the western part of the storm track can be attributed to the strong baroclinicity that dominates in these regions during the cold season. The permanent and pronounced baroclinic forcing results in a regular and fast production of waves.

b. Poisson regression

Maximum likelihood estimates of the 10 regression parameters β_k, $k = 1, \ldots, 10$ (each corresponding to one teleconnection pattern) are plotted in Fig. 8 for the Atlantic and Europe, and in Fig. 9 for the Pacific and North America (the estimation is discussed in the appendix). Regions where there is overwhelming evidence that the β_k parameters are different from zero (very stringent significance level of 0.1%) are shaded in gray. High transit rates are associated with low pressure regions in the teleconnection patterns. All teleconnection patterns in Fig. 8 are necessary for explaining the variations in monthly cyclone counts observed in the northeastern Atlantic and Europe. The NAO contribution (Fig. 8a) is significant at the 0.1% level across a large area extending from northern Canada to Iceland and northern Europe (more particularly Scandinavia), and also south of the North Atlantic storm track and in southern Europe. In high-latitude regions, higher (lower) monthly cyclone counts are associated with a positive (negative) phase of the NAO. Farther south, lower (higher) monthly cyclone counts are associated with a positive (negative) phase of the NAO. A striking feature of Fig. 8a is the white corridor region along the southern part of the North Atlantic storm track and into France–Germany. In this zone the NAO regression coefficient is not significantly different from zero at the 0.1% level (i.e., the NAO has less or little impact on the observed monthly cyclone counts). Although it is generally accepted that the NAO modulates the frequency of cyclone occurrences in the North Atlantic and western Europe, Fig. 8a shows that the NAO alone does not explain the whole variability of cyclone counts everywhere in or near the North Atlantic storm track. Figure 8b provides evidence that the variability not accounted for by the NAO in the southeastern section of the storm track can be largely explained by the east Atlantic pattern (EAP). During positive EAP, cyclones tend to track south of the normal storm-track position. The area coincides with the region of secondary cyclogenesis identified by Dacre (2005). This suggests that the variations in cyclone counts in this region are at least partly caused by changes in the cyclogenesis activity. Bishop and Thorpe (1994a,b) and Dacre (2005) showed how modulations of the frontogenetic strain can trigger or inhibit wave instability. The EAP is associated with this kind of flow deformation. Figure 8c shows that a positive (negative) phase of the Scandinavian pattern (SCP) is a major explanatory factor for decreased (increased) cyclone counts in northern Europe and Rus-

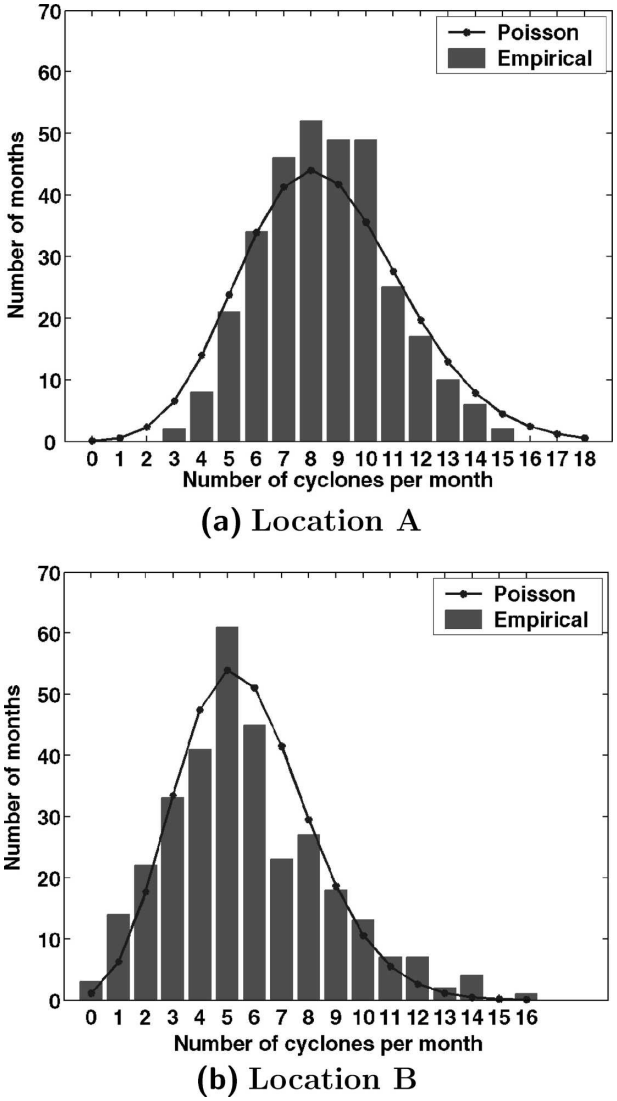

FIG. 7. Histograms of monthly transit counts in locations A and B for all 53 winters. The curves show the corresponding Poisson distributions that were fitted using the sample means.

sia. A positive phase of the SCP corresponds to a blocking high above northern Europe, a weak storm track deflected far to the north of its usual position, and often cyclonic features cut off from the main circulation hanging in the southwest. Similarly positive (negative) phases of the east Atlantic–western Russian pattern correspond to spells of anomalously high (low) pressure and reduced (increased) cyclone counts above western Europe except the Arctic region (Fig. 8d). Positive (negative) phases of the polar–Eurasian pattern, which are associated with a deeper-than-normal (shallower than normal) polar vortex and higher-than-normal (lower than normal) pressure values over Eurasia, also account for reduced (increased) cyclone counts across southern Europe, and for increased (reduced) cyclone counts in northern Europe and nearly the whole Arctic region (Fig. 8e).

In its positive phase, the Pacific–North American pattern (PNA) is associated with a stronger-than-normal Hawaiian high, a deeper-than-normal Aleutian low, positive pressure anomalies in northwestern America, and negative pressure anomalies in the southeast of the United States and in the Gulf of Mexico. This is reflected by a decrease in cyclone counts across the Canadian west coast, and an increase in cyclone counts in the North Pacific as well as in the Gulf of Mexico and the Caribbean (Fig. 9a). The North Pacific pattern, which is also associated with the relative strengths of the subtropical Pacific anticyclone and the Aleutian low, affects cyclone counts in a way similar to the PNA (Fig. 9d). Notice that in the case of the North Pacific pattern, the β_k parameter does not reach statistical significance at the 0.1% level. This is due to the pattern being active only one month out of six (March). The dipole structures of the west and east Pacific patterns are also visible in Figs. 9b,c. Finally, the structure of the tropical Northern Hemisphere pattern can also be recognized in Fig. 9e.

c. Residual dispersion

Figure 10 shows the estimated dispersion $\hat{\psi}$ that takes into account the variability of μ in the Poisson regression instead of assuming constant μ (residual dispersion),

$$\hat{\psi} = \frac{1}{m - p - 1} \sum_{i=1}^{m} \frac{(n_i - \hat{\mu}_i)^2}{\hat{\mu}_i} - 1, \qquad (2)$$

where n_i is the observed transit count in month i, and $\hat{\mu}_i$ is the estimate of the mean transit count for month i given by Eq. (A4). The summation is over $m = 318$ months, and $p = 15$ is the number of regression parameters.

In the regression, the explanatory variables x_k represent the mean state of the large-scale atmospheric flow for each month summarized by 10 teleconnection patterns plus 5 extra binary indicators to account for monthly variations due to seasonality. However, the x_k variables also contain fluctuations that have shorter time scales than 1 month. For instance, the NAO can stay in a moderate positive phase (cyclone counts slightly larger than average in northern Europe) for 1 week, then move to a strong negative phase (counts much smaller than average) for 2 weeks, and then neutral (normal counts) for 1 week. The net monthly average for the month in this case is negative (there are less cyclones than usual). Regression removes the effect

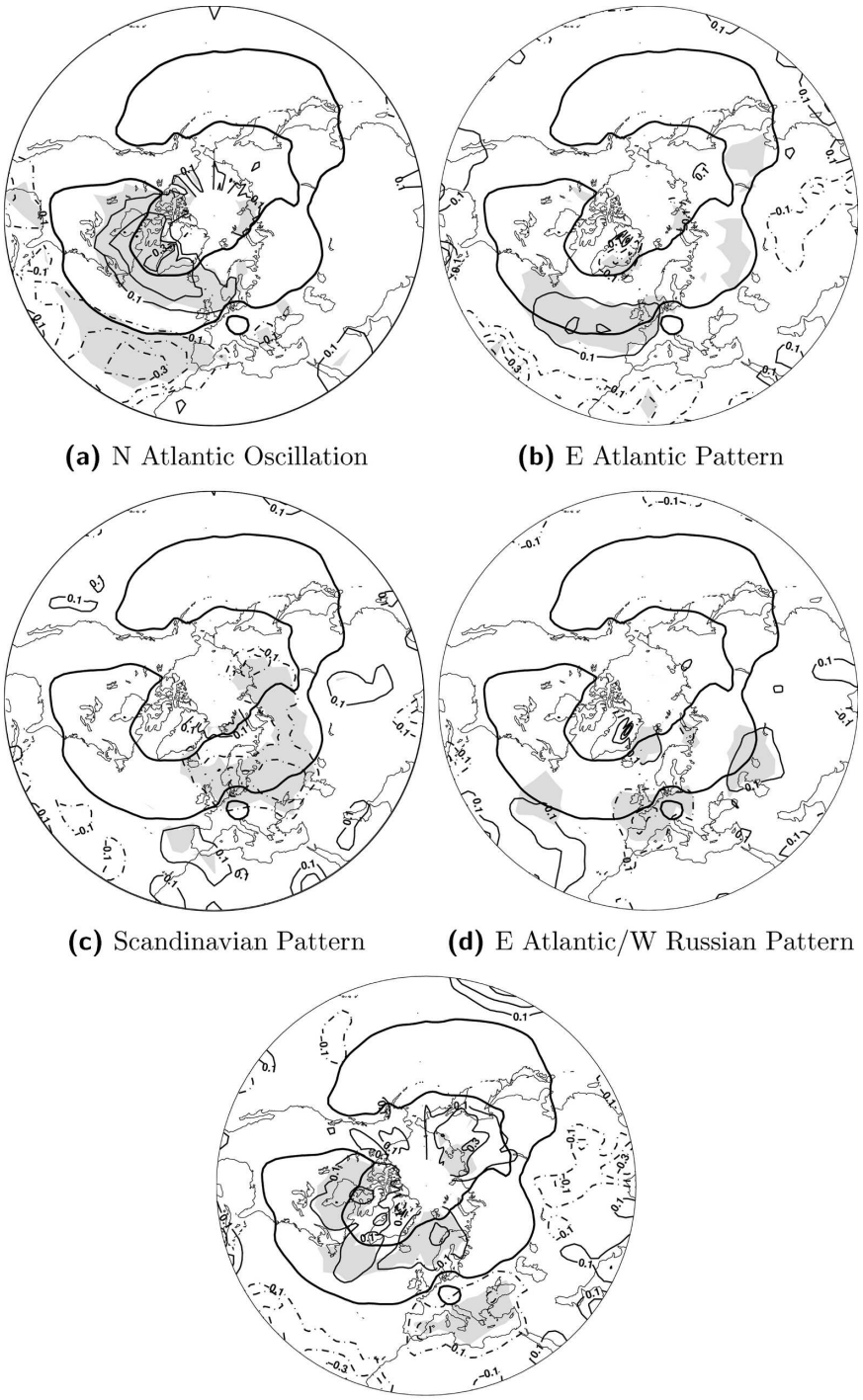

FIG. 8. Estimates of the β_k parameters for the five teleconnection patterns relevant for the North Atlantic and Europe. Solid (dashed) lines indicate positive (negative) values. Contours start at ± 0.1, contour intervals of 0.2. Areas with p values $\leq 10^{-3}$ are shaded.

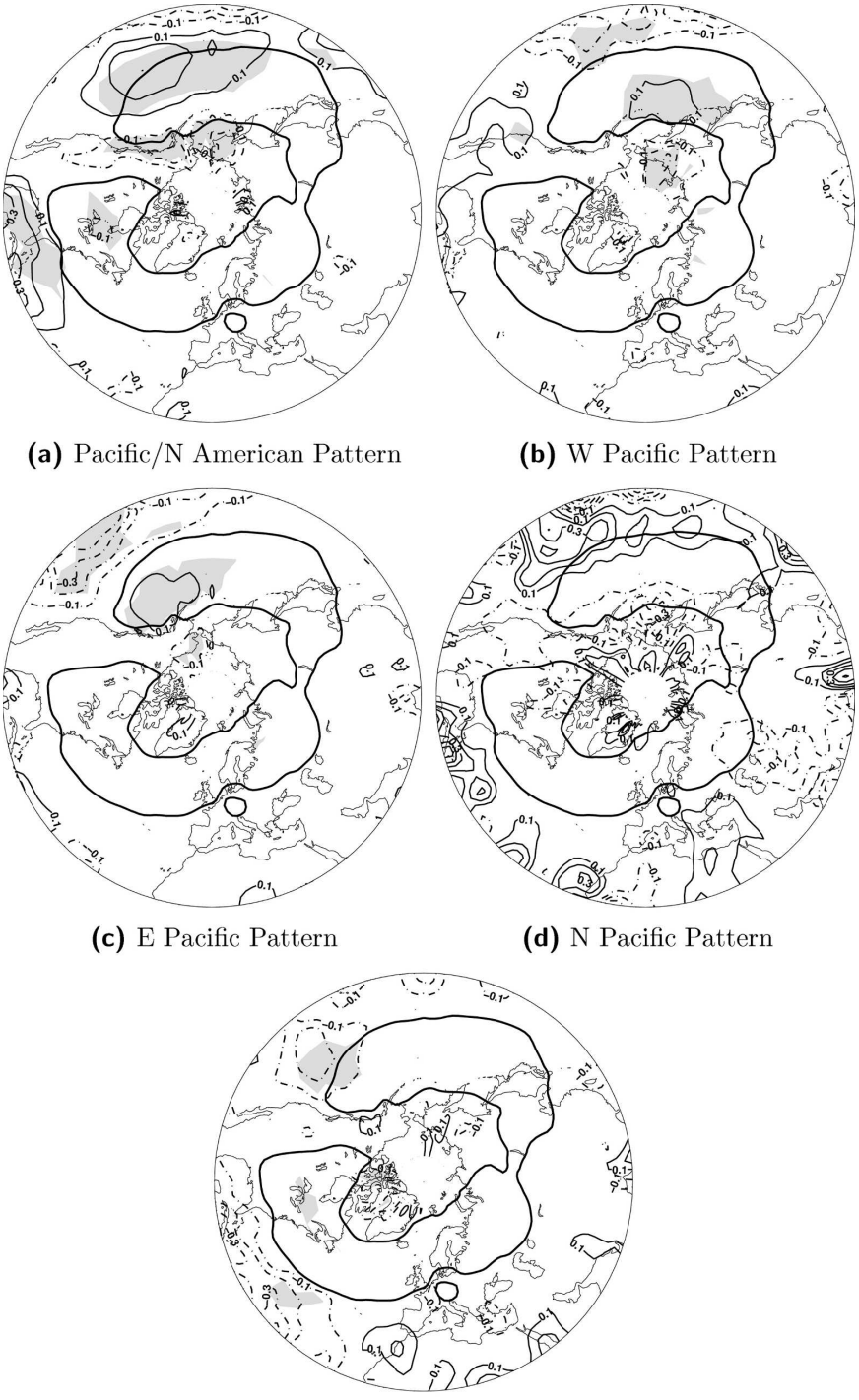

FIG. 9. Estimates of the β_k parameters for the five teleconnection patterns relevant for the North Pacific and North America. Contouring and shading is the same as in Fig. 8.

of all these intramensual variations on monthly counts altogether. The remaining (residual) dispersion is due to variability that is not accounted for by the teleconnection patterns or seasonality. Baroclinic waves are the principal source of such variability in the storm tracks. As the regression coefficients are the same for all years, some variability may also remain owing to effects that are on time scales longer than a year, but

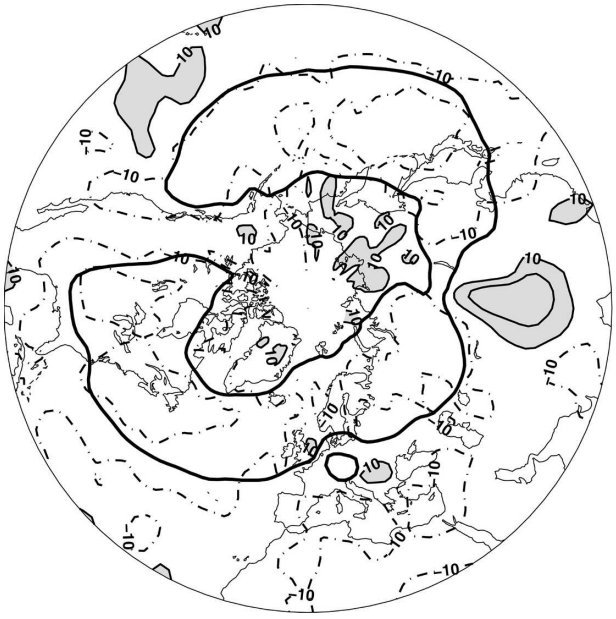

FIG. 10. Estimated residual dispersion of the monthly number of cyclone transits. Contouring and shading is the same as in Fig. 5.

these effects have been assumed to be negligible in the context of this study. In Fig. 10, negative values predominate in the North Atlantic and North Pacific storm tracks. These negative values indicate statistically significant underdispersion, which is consistent with regularity due to undisturbed baroclinic wave trains.

d. Dispersion and system intensity

The results discussed above are based on the complete set of tracks in the database. Not all systems considered in this analysis develop into major storms. However, since society in general and reinsurers in particular are more interested in intense extratropical cyclones, it is pertinent to look into a possible association between clustering and system strength. Figure 11a shows the estimated dispersion $\hat{\psi}$ (assuming μ is constant) when the weakest features ($\xi_{850} < 6 \times 10^{-5}\ \mathrm{s}^{-1}$) are eliminated. Figure 11b, on the other hand, shows $\hat{\psi}$ after removing the strongest features ($\xi_{850} \geq 6 \times 10^{-5}\ \mathrm{s}^{-1}$). Figure 11a is qualitatively more similar to Fig. 5 in the northeast Atlantic, Europe (dashed rectangle E in Fig. 11a), and in the central North Pacific (dashed rectangle P), suggesting that serial clustering in these regions tends to be associated with systems of more significant intensity. Overdispersion in Europe is even greater in Fig. 11a ($\hat{\psi} \geq 50\%$ in the North Sea). In contrast, Fig. 11b is qualitatively more similar to Fig. 5 over central and southwest Asia (dashed rectangle A in Fig. 11b). The blank space over Asia in Fig. 11a indicates that overdispersion in these areas is associated with weaker features of $\xi_{850} < 6 \times 10^{-5}\ \mathrm{s}^{-1}$.

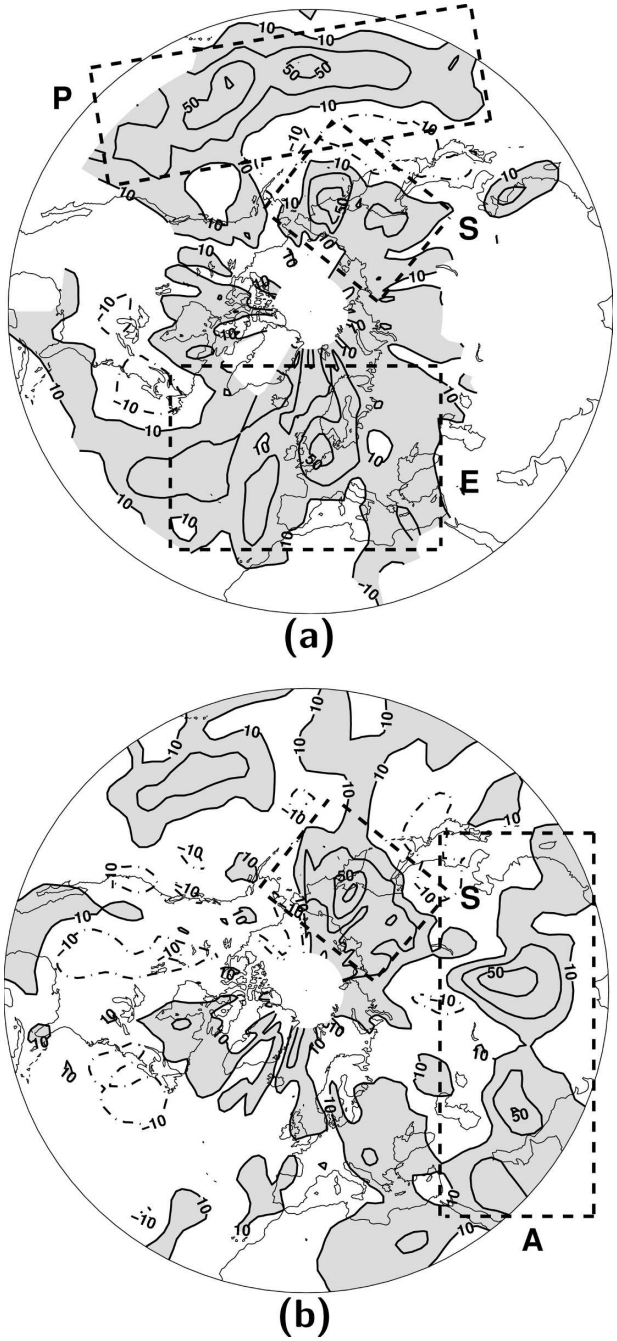

FIG. 11. Estimated dispersion for the (a) strongest and (b) weakest cyclones (threshold value for $\xi_{850} = 6 \times 10^{-5}\ \mathrm{s}^{-1}$). Contouring and shading is the same as in Fig. 5.

Overdispersion in northeastern Siberia and Kamchatka (dashed rectangles S in Fig. 11) involves cyclones of both categories.

e. Predictability

The potential use of time-lagged monthly teleconnection indices to predict future variations in cyclone counts was also considered. Poisson regression was performed again on the same track data, this time using 1-month-lagged teleconnection indices. The residual dispersion is shown in Fig. 12. Regression on 1-month-lagged indices does not remove much of the overdispersion in the eastern North Atlantic and Europe. It does, however, remove a significant part of the overdispersion in the central Pacific, and in northeastern and southwestern Asia. The apparently better performance of 1-month-lagged indices over the latter regions is mainly a statistical artifact due to indices being set to zero for consecutive months when the corresponding teleconnection patterns are inactive (Table 1). Where teleconnection patterns are active from October to March, time-lagged indices do not have much predictive skill because of their limited persistence 1 month ahead. It must be pointed out though, that this method of prediction is very crude, and that time-lagged indices can be reasonably expected to show more skill in the medium and extended ranges (3–30 days).

Finally, the statistical analysis conducted here does not discriminate between causes and effects, and future work on the prediction of serial clustering will need to address this issue.

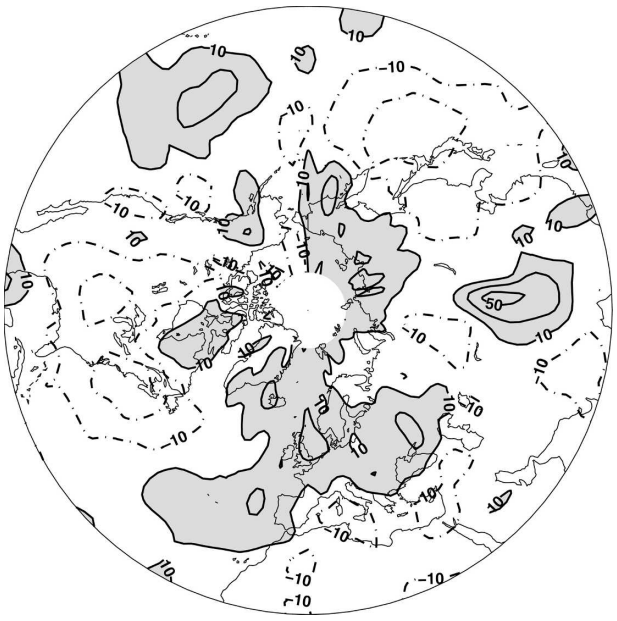

FIG. 12. Estimated residual dispersion of the monthly number of cyclone transits using 1-month-lagged teleconnection indices as explanatory variables. Contouring and shading is the same as in Fig. 5.

6. Conclusions

This study has investigated the clustering in time (seriality) of extratropical cyclones in the Northern Hemisphere.

A long database of cyclone tracks over the Northern Hemisphere has been created for 53 consecutive extended winters (from October to March) from 1950 to 2003. The analysis has used tracks based on maxima of low-level relative vorticity (ξ_{850}) that allow better cyclone detection than minima of mean sea level pressure.

A point-process approach was then used to investigate local variations in the monthly cyclone counts. The coefficient of dispersion of the monthly cyclone counts was used to quantify serial clustering. An extensive region of statistically significant overdispersion—more serial clustering than expected due to chance—was identified in the exit region of the North Atlantic storm track, Europe, and the central North Pacific. The clustering in the northeastern Atlantic and Europe is similar for cyclones of higher intensity ($\xi_{850} \geq 6 \times 10^{-5}$ s^{-1}). In contrast, there is little evidence of clustering to the west of North America. The very high rates and pronounced regularity (underdispersion) in the entrance regions of the North Pacific and North Atlantic storm tracks are most likely due to the permanent baroclinic forcing that prevails in these regions.

A Poisson regression model has been used to show that the variation of monthly cyclone counts is largely accounted for by modes of climate variability with lower frequencies than the synoptic scale. Five independent teleconnection patterns were found to be important for Europe: The NAO, EAP, SCP, the east Atlantic–western Russian pattern, and the polar–Eurasian pattern. The NAO alone is not sufficient to account for the variability of cyclone rates in the North Atlantic and western Europe. The residual variation of cyclone counts for the North Atlantic and North Pacific storm tracks shows significant underdispersion associated with a regular procession of undisturbed baroclinic waves.

This study has identified two distinct mechanisms for serial clustering:

- The variability of the large-scale pattern controls the speed and path of existing cyclones. For instance, a highly positive (negative) NAO index is associated with a sharp (slack) baroclinic gradient, a vigorous (weak) upper-level jet stream across the North Atlantic, and fast (slow) transients moving northeastward (eastward). In situations with a blocking high

over the north of Europe (e.g., positive SCP index and negative NAO index), cyclones are slowed down, weakened, and diverted away from the north of Europe. This form of clustering can be better appreciated by considering an analogy with traffic flow. It is well known in the United Kingdom that buses tend to arrive at bus stops in clusters separated by long periods when no buses arrive. This is primarily because their arrival rates are controlled by variations in traffic flow. Buses leave the depot at regular intervals (regular point process) but then the buses get delayed by time-varying amounts as they cross towns and cities. The clustering observed at point locations (e.g., bus stops) is a natural consequence of the time-varying rate dependence. Similar clustering should be expected to occur with extratropical cyclones, which are generated at regular intervals at the western ends of the Atlantic and Pacific storm tracks and then make their way across each ocean basin. An additional subtlety of weather systems not present with buses is that they can also modify their routes as they cross the domain. This mechanism for serial clustering is best modeled with a point process with a variable rate.

- The variability of the large-scale pattern also generates regions where new cyclones are formed. Regions under the right entrance and left exit of jet streams are prone to cyclogenesis. Furthermore, a positive phase of the EAP can be associated with cyclogenesis through relaxation of the baroclinic gradient in the eastern North Atlantic. A traffic analogy to this mechanism is the occasional arrival and insertion of new vehicles on the road (either alone or in groups). This mechanism is in essence a cluster process, but in the Poisson regression model it has been implicitly considered as equivalent to a point process with a variable rate.

A stratification of cyclones into strong and weak features using a relative vorticity threshold of $6 \times 10^{-5}\ \mathrm{s}^{-1}$ has revealed that serial clustering of cyclones in the northeast Atlantic, Europe, and in the central North Pacific is more particularly associated with the strong systems.

The predictive skill of 1-month-lagged teleconnection indices were briefly assessed and found to be limited due to their lack of persistence. The analysis performed in this study does not allow us to discriminate causes from effects, and more work is required to better understand the mechanisms of serial clustering and examine its predictability.

The work presented in this paper has dealt exclusively with the serial clustering of extratropical cyclones. We suggest that a similar point-process approach could be extended in future to investigate the serial properties of other weather systems such as tropical cyclones, tornadoes, and polar lows.

Acknowledgments. This work was funded by the Risk Prediction Initiative of the Bermuda Biological Station for Research (Project H1423900) and is part of the Ph.D. dissertation of P. J. Mailier at the University of Reading, United Kingdom (Natural Research Council Award NER/S/S/2001/06731A). The authors thank Rick Murnane and the RPI consortium for useful feedback. We are also grateful to Mathew Sapiano and Ivar Seierstad for their help with the graphics, and to Sevim Müller of the Team Wetterpate at the Freie Universität Berlin for kindly providing information on the names of European cyclones. Three anonymous reviewers are also acknowledged for the comments and suggested changes that have helped improve the quality of this manuscript.

APPENDIX

Poisson Process and Poisson Regression

a. The Poisson process

The one-dimensional Poisson process (Cox and Isham 1980) is a stochastic point process that models the occurrence of random events in time. The *rate parameter* λ of the process has units of inverse time and is sometimes referred to as the *intensity* of the process. The homogeneous one-dimensional Poisson process is the simplest model to describe *complete serial randomness*. It has constant rate λ. The Poisson process is defined by three basic randomness postulates.

1) The probability that exactly one event occurs in any small time interval $[t, t + \delta t]$ is equal to $\lambda\delta t + o(\delta t)$, where $o(\delta t)$ tends to zero faster than δt in the limit as δt tends to zero.
2) The probability that two or more events occur in any small time interval $[t, t + \delta t]$ is equal to $o(\delta t)$—in other words, is very small compared to the probability of one event occurring.
3) The occurrence of events after any time t is independent of the occurrence of events before time t.

With constant rate λ, the number N of events during any time interval of length Δt has a Poisson distribution with mean and variance $\mu = \lambda\Delta t$. The probability of $N = n$ events during the interval is given by

$$P(N = n) = \frac{(\lambda\Delta t)^n e^{-\lambda\Delta t}}{n!}, \quad n = 0, 1, 2, \ldots. \qquad \text{(A1)}$$

The *index of dispersion* ϕ for N is given by

$$\phi = \frac{\mathrm{Var}(N)}{E(N)}, \tag{A2}$$

where $E(N)$ and $\mathrm{Var}(N)$ are the mean and the variance of N, respectively.

For a homogeneous Poisson process, $\phi = 1$. When $\phi > 1$, the process is more clustered than random. When $\phi < 1$, the process is more regular than random. For this study we also introduce the dispersion statistic $\psi = \phi - 1$. In the case of a clustered pattern $\psi > 0$ (overdispersion), whereas for a regular pattern $\psi < 0$ (underdispersion).

b. Poisson regression

The inhomogeneous one-dimensional Poisson process has a rate $\lambda(t)$ that varies with time. The counts N can be modeled using *Poisson regression.* This class of generalized linear model (McCullagh and Nelder 1989, chapter 6) uses a logarithmic link function to relate $\ln(\mu)$ to a linear combination of explanatory variables x_k. Given fixed values of μ, the number of events N is assumed to be Poisson distributed:

$$N \,|\, \mu \sim \mathrm{Poisson}(\mu), \tag{A3}$$

$$\ln(\mu) = \beta_0 + \sum_{k=1}^{p} \beta_k x_k. \tag{A4}$$

Equation (A3) must be read "N given μ is Poisson distributed with mean μ." Maximum-likelihood estimates $\hat{\beta}_k$ of the regression parameters β_k can be obtained by means of an iterative weighted least squares algorithm. For this study, the MATLAB function *glmfit* was used.

For variable μ, it can be shown that

$$E(N) = E(\mu) \tag{A5}$$

$$\mathrm{Var}(N) = E(\mu) + \mathrm{Var}(\mu). \tag{A6}$$

Hence, the dispersion index is given by

$$\phi = 1 + \frac{\mathrm{Var}[\exp(\beta_0 + \beta_1 x_1 + \ldots + \beta_p x_p)]}{E[\exp(\beta_0 + \beta_1 x_1 + \ldots + \beta_p x_p)]}, \tag{A7}$$

that is, for a Poisson process with variable μ and logarithmic link, the index of dispersion is always greater than 1.

c. Dispersion

An estimate of the index of dispersion ϕ that removes inflation caused by monthly fluctuations of μ is

$$\hat{\phi} = \frac{1}{m - p - 1} \sum_{i=1}^{m} \frac{(n_i - \hat{\mu}_i)^2}{\hat{\mu}_i}. \tag{A8}$$

In this study $m = 318$ is the total number of months, n_i is the observed monthly transit count in the ith month, $\hat{\mu}_i$ is the estimate of the mean transit count during the ith month, and $p = 15$ is the number of regression parameters. Under the hypothesis that μ is constant ($p = 0$), Eq. (A8) becomes

$$\hat{\phi} = \frac{1}{m - 1} \sum_{i=1}^{m} \frac{(n_i - \hat{\mu})^2}{\hat{\mu}}, \tag{A9}$$

$$= \frac{s_n^2}{\bar{n}}, \tag{A10}$$

where $\bar{n}$ is the sample mean, and s_n^2 the sample variance of the 318 monthly totals n_i of cyclone transits.

If N is Poisson distributed, then the Pearson statistic $X^2 = (m - p - 1)\hat{\phi}$ is approximately χ^2 distributed with $\upsilon = (m - p - 1)$ degrees of freedom. If the number of degrees of freedom is sufficiently large ($\upsilon > 200$), the normal approximation to the χ^2 distribution may be used by invoking the Central Limit Theorem. Then, X^2 is approximately normally distributed with mean $(m - p - 1)$ and variance $2(m - p - 1)$.

REFERENCES

Akyildiz, V., 1985: Systematic errors in the behaviour of cyclones in the ECMWF operational models. *Tellus,* **37A,** 297–308.

Anderson, D., K. I. Hodges, and B. J. Hoskins, 2003: Sensitivity of feature-based analysis methods of storm tracks to the form of background field removal. *Mon. Wea. Rev.,* **131,** 565–573.

Barnston, A. G., and R. E. Livezey, 1987: Classification, seasonality, and persistence of low-frequency atmospheric circulation patterns. *Mon. Wea. Rev.,* **115,** 1083–1126.

Bergeron, T., 1954: The problem of tropical hurricanes. *Quart. J. Roy. Meteor. Soc.,* **80,** 131–164.

Bishop, C. H., and A. J. Thorpe, 1994a: Frontal wave stability during moist deformation frontogenesis. Part I: Linear wave dynamics. *J. Atmos. Sci.,* **51,** 852–873.

——, and ——, 1994b: Frontal wave stability during moist deformation frontogenesis. Part II: The suppression of nonlinear wave development. *J. Atmos. Sci.,* **51,** 874–888.

Bjerknes, J., and H. Solberg, 1922: Life cycle of cyclones and the polar front theory of atmospheric circulation. *Geofys. Publ.,* **3,** 3–18.

Blender, R., K. Fraedrich, and F. Lunkheit, 1997: Identification of cyclone track regimes in the North Atlantic. *Quart. J. Roy. Meteor. Soc.,* **123,** 727–741.

Chang, E., and I. Orlanski, 1993: On the dynamics of a storm track. *J. Atmos. Sci.,* **50,** 999–1015.

——, and ——, 1994: On energy flux and group velocity of waves in baroclinic flows. *J. Atmos. Sci.,* **51,** 3823–3828.

Charney, J. G., 1947: The dynamics of long waves in a baroclinic westerly current. *J. Meteor.,* **4,** 135–163.

Cox, D. R., and V. Isham, 1980: *Point Processes.* Chapman and Hall/CRC, 188 pp.

Dacre, H., 2005: Frontal waves. Ph.D. thesis, University of Reading, 134 pp.

Deveson, A. C. L., K. A. Browning, and T. D. Hewson, 2002: A classification of FASTEX cyclones using a height-attributable quasi-geostrophic vertical-motion diagnostic. *Quart. J. Roy. Meteor. Soc.,* **128,** 93–117.

Eady, E. T., 1949: Long waves and cyclone waves. *Tellus,* **1,** 33–52.

Eliassen, A., 1966: Motions of intermediate scales: Fronts and cyclones. *Advances in Earth Science,* E. D. Hurley, Ed., MIT Press, 111–138.

Goldfarb, D., 1969: Extension of Davidon's variable metric method to maximization under linear inequality and equality constraints. *SIAM J. Appl. Math.,* **17,** 739–764.

Hodges, K. I., 1994: A general method for tracking analysis and its application to meteorological data. *Mon. Wea. Rev.,* **122,** 2573–2586.

——, 1995: Feature tracking on the unit sphere. *Mon. Wea. Rev.,* **123,** 2914–2932.

——, 1996: Spherical nonparametric estimators applied to the UGAMP model integration for AMIP. *Mon. Wea. Rev.,* **124,** 2914–2932.

——, 1999: Adoptive constraints for feature tracking. *Mon. Wea. Rev.,* **127,** 1362–1373.

——, B. J. Hoskins, J. Boyle, and C. Thorncroft, 2003: A comparison of recent reanalysis datasets using objective feature tracking: Storm tracks and tropical easterly waves. *Mon. Wea. Rev.,* **131,** 2012–2037.

Hoskins, B. J., and P. J. Valdes, 1990: On the existence of storm tracks. *J. Atmos. Sci.,* **47,** 1854–1864.

——, and K. I. Hodges, 2002: New perspectives on the northern hemisphere winter storm tracks. *J. Atmos. Sci.,* **59,** 1041–1061.

Kalnay, E., and Coauthors, 1996: The NCEP/NCAR 40-Year Reanalysis Project. *Bull. Amer. Meteor. Soc.,* **77,** 437–471.

Klein, W. H., 1957: Principal tracks and mean frequencies of cyclones and anti-cyclones in the Northern Hemisphere. Research Paper 40, U.S. Weather Bureau, Washington, DC, 60 pp.

Lim, E.-P., and I. Simmonds, 2002: Explosive cyclone development in the Southern Hemisphere and a comparison with Northern Hemisphere events. *Mon. Wea. Rev.,* **130,** 2188–2209.

Mallet, I., J. P. Cammas, P. Mascart, and P. Bechtold, 1999: Effects of cloud diabatic heating on the early development of the FASTEX IOP17 cyclone. *Quart. J. Roy. Meteor. Soc.,* **125,** 3439–3467.

McCullagh, P., and J. A. Nelder, 1989: *Generalized Linear Models.* 2d ed. Chapman and Hall, 511 pp.

Munich Re, 2002: Winter storms in Europe (II). Analysis of 1999 losses and loss potentials. Rep. 302-03109, 72 pp. [Available from Münchener Rückversicherungs-Gesellschaft, Königinstrasse 107, 80802 München, Germany.]

Murray, R., and S. M. Daniels, 1953: Transverse flow at entrance and exit to jet streams. *Quart. J. Roy. Meteor. Soc.,* **79,** 236–241.

Murray, R. J., and I. Simmonds, 1991: A numerical scheme for tracking cyclone centres from digital data. Part I: Development and operation of the scheme. *Aust. Meteor. Mag.,* **39,** 155–166.

Namias, J., and P. F. Clapp, 1949: Confluence theory of the high tropospheric jet stream. *J. Meteor.,* **6,** 330–336.

Orlanski, I., and E. K. M. Chang, 1993: Ageostrophic geopotential fluxes in downstream and upstream development of baroclinic waves. *J. Atmos. Sci.,* **50,** 212–225.

Palmén, E., and C. W. Newton, 1969: *Atmospheric Circulation Systems: Their Structure and Physical Interpretation.* International Geophysics Series, Vol. 13, Academic Press, 603 pp.

Panagiotopoulos, F., M. Shahgedanova, and D. B. Stephenson, 2002: A review of Northern Hemisphere wintertime teleconnection patterns. *J. Phys. IV,* **12,** 27–47.

Parker, D. J., 1998: Secondary frontal waves in the North Atlantic region: A dynamical perspective of current ideas. *Quart. J. Roy. Meteor. Soc.,* **124,** 829–856.

Petterssen, S., 1956: *Weather Analysis and Forecasting.* Vol. 1, 2d ed., McGraw-Hill, 428 pp.

——, and S. J. Smebye, 1971: On the development of extratropical cyclones. *Quart. J. Roy. Meteor. Soc.,* **97,** 457–482.

Reed, R. J., A. Hollingsworth, W. A. Heckley, and F. Delsol, 1986: An evaluation of the performance of the ECMWF operational forecasting system in analyzing and forecasting tropical easterly wave disturbances. Part I: Synoptic investigation. ECMWF Tech. Rep. 58, 96 pp.

Renfrew, I. A., A. J. Thorpe, and C. Bishop, 1997: The role of environmental flow in the development of secondary frontal cyclones. *Quart. J. Roy. Meteor. Soc.,* **123,** 1653–1676.

Roebber, P. J., 1984: Statistical analysis and updated climatology of explosive cyclones. *Mon. Wea. Rev.,* **112,** 1577–1589.

Rogers, J. C., 1997: North Atlantic storm track variability and its association to the North Atlantic Oscillation and climate variability of northern Europe. *J. Climate,* **10,** 1635–1647.

Sanders, F., and J. R. Gyakum, 1980: Synoptic-dynamic climatology of the "Bomb." *Mon. Wea. Rev.,* **108,** 1589–1606.

Serreze, M. C., 1995: Climatological aspects of cyclone development and decay in the Arctic. *Atmos.–Ocean,* **33,** 1–23.

——, F. Carse, R. G. Barry, and J. C. Rogers, 1997: Icelandic low cyclone activity: Climatological features, linkages with the NAO, and relationships with recent changes in the Northern Hemisphere circulation. *J. Climate,* **10,** 453–464.

Simmonds, I., and K. Keay, 2000: Mean Southern Hemisphere extratropical cyclone behavior in the 40-year NCEP–NCAR reanalysis. *J. Climate,* **13,** 873–885.

——, R. J. Murray, and R. M. Leighton, 1999: A refinement of cyclone tracking methods with data from FROST. *Aust. Meteor. Mag.,* June Special Edition, 35–49.

Simmons, A. J., and B. J. Hoskins, 1979: The downstream and upstream development of unstable baroclinic waves. *J. Atmos. Sci.,* **36,** 1239–1254.

Sinclair, M. R., 1994: An objective cyclone climatology for the Southern Hemisphere. *Mon. Wea. Rev.,* **122,** 2239–2256.

Thorncroft, C. D., and B. J. Hoskins, 1990: Frontal cyclogenesis. *J. Atmos. Sci.,* **47,** 2317–2336.

Uccellini, L. W., 1990: Processes contributing to the rapid development of extratropical cyclones. *Extratropical Cyclones: The Erik Palmén Memorial Volume,* C. N. Newton and E. O. Holopainen, Eds., Amer. Meteor. Soc., 81–105.

——, and D. R. Johnson, 1979: The coupling of upper and lower tropospheric jet streaks and implications for the development of severe convective storms. *Mon. Wea. Rev.,* **107,** 682–703.